

Article

Satellite Sensed Data-Dose Response Functions: A Totally New Approach for Estimating Materials' Deterioration from Space

Georgios Kouremadas ^{1,*}, John Christodoulakis ^{1,2} , Costas Varotsos ¹  and Yong Xue ^{3,4}

¹ Climate Research Group, Section of Environmental Physics and Meteorology, Faculty of Physics, National & Kapodistrian University of Athens, GR-15784 Athens, Greece; ichristodoulakis@acg.edu (J.C.); covar@phys.uoa.gr (C.V.)

² Department of Science and Mathematics, School of Liberal Arts and Sciences, The American College of Greece, GR-15342 Aghia Paraskevi, Greece

³ Emergency Management College, Nanjing University of Information Science & Technology, Nanjing 210044, China; yxue@nuist.edu.cn

⁴ Department of Electronics, Computing and Mathematics, College of Science & Engineering, University of Derby, Derby DE22 1GB, UK

* Correspondence: gkoure@phys.uoa.gr

Abstract: When construction materials are exposed to the atmospheric environment, they are subject to deterioration, which varies according to the time period of exposure and the location. A tool named Dose–Response Functions (DRFs) has been developed to estimate this deterioration. DRFs use specific air pollutants and climatic parameters as input data. Existing DRFs in the literature use only ground-based measurements as input data. This fact constitutes a limitation for the application of this tool because it is too expensive to establish and maintain such a large network of ground-based stations for pollution monitoring. In this study, we present the development of new DRFs using only satellite data as an input named Satellite Sensed Data Dose-Response Functions (SSD-DRFs). Due to the global coverage provided by satellites, this new tool for monitoring the corrosion/soiling of materials overcomes the previous limitation because it can be applied to any area of interest. To develop SSD-DRFs, we used measurements from MODIS (Moderate Resolution Imaging Spectroradiometer) and AIRS (Atmospheric Infrared Sounder) on board Aqua and OMI (Ozone Monitoring Instrument) on Aura. According to the obtained results, SSD-DRFs were developed for the case of carbon steel, zinc, limestone and modern glass materials. SSD-DRFs are shown to produce more reliable corrosion/soiling estimates than “traditional” DRFs using ground-based data. Furthermore, research into the development of the SSD-DRFs revealed that the different corrosion mechanisms taking place on the surface of a material do not act additively with each other but rather synergistically.

Keywords: satellite data; corrosion; soiling; modeling corrosion tools; machine learning



Citation: Kouremadas, G.; Christodoulakis, J.; Varotsos, C.; Xue, Y. Satellite Sensed Data-Dose Response Functions: A Totally New Approach for Estimating Materials' Deterioration from Space. *Remote Sens.* **2023**, *15*, 3194. <https://doi.org/10.3390/rs15123194>

Academic Editor: Daniele Bortoli

Received: 7 May 2023

Revised: 8 June 2023

Accepted: 15 June 2023

Published: 20 June 2023



Copyright: © 2023 by the authors. Licensee MDPI, Basel, Switzerland. This article is an open access article distributed under the terms and conditions of the Creative Commons Attribution (CC BY) license (<https://creativecommons.org/licenses/by/4.0/>).

1. Introduction

When various materials are exposed to the air we breathe, they suffer wear and tear from both air quality and the wind depending on the time of exposure and location. To deal with this problem, maintenance procedures are used, which constitute 4–5% of the global GDP (gross domestic product) [1]. The role of air pollution, in relation to climatic conditions, in the deterioration of construction materials exposed outdoors has already been recognized in the literature [2–6]. To model this deterioration, a tool named Dose–Response Function (DRF) has been developed. Firstly, this tool was developed after laboratory deterioration experiments in a controlled environment. Before the 2000s, it was found that the main air pollutant dominating the corrosion/soiling effect was SO₂. So, the main research focused on the effect of SO₂ on different materials. The presence of additional contaminants in the atmospheric environment has led to the study of their participation in the corrosion/soiling effect on materials such as SO₂. After several studies, it was shown

that NO_2 and O_3 contribute to corrosion/the soiling effect. The difference is that there is no direct chemical reaction with materials, but their presence on the surface of the material has a catalytic reaction with the presence of SO_2 . After the 2000s, with the desulfurization of the atmosphere, it was seen that the corrosion/soiling problem was a multi-factorial effect [7–19]. Nowadays, DRFs quantify the corrosion/soiling effect on materials using the concentration of specific air pollutants, such as SO_2 , NO_2 , O_3 , HNO_3 , PM_{10} (particulate matter with an aerodynamic diameter equal to or less than $10\text{ }\mu\text{m}$) and meteorological parameters such as temperature, relative humidity and precipitation [20–27].

Over the years, several projects have been carried out with exposure campaigns to develop new DRFs or improve existing ones. One of these projects with a significant contribution to this effort is called the “International Co-operative Programme on Effects on Materials including Historic and Cultural Monuments (ICP Materials)”. In this study, we use some of the DRFs developed in the framework of ICP Materials, specifically for the materials carbon steel, zinc, limestone and modern glass [23,28]. The common characteristic of all existing DRFs in the literature is that they use ground-based measurements of air pollutants and meteorological parameters. This feature limits their application to cases where the necessary ground-based data are available.

This research attempts to overcome this limitation by developing new deterioration modeling tools that make use of satellite data that have the advantage of near-global coverage. Such satellite data are recorded by remote sensing instruments on environmental satellites. All these available satellite data can be used in material deterioration modeling.

This study presents the development of these new deterioration modeling tools that use satellite data to quantify corrosion/soiling in structural materials. To identify these new DRFs, the term Satellite-Sensed Data Dose–Response Functions or SSD-DRFs is proposed.

2. Materials and Methods

2.1. Object of Study

The materials studied in this research are the following:

- Carbon steel;
- Zinc;
- Limestone;
- Modern glass.

These materials were chosen because they are widely used in modern constructions. Additionally, limestone and zinc are the basic materials in cultural heritage monuments. Within the framework of the ICP Materials and MULTI-ASSESS (model for multi-pollutant impact and assessment of threshold levels for cultural heritage) projects, DRFs were developed for each material. These DRFs are presented below ([23] Equations (1)–(3); [28] Equation (4)):

DRFs.

Carbon steels

$$ML = 51 + 1.39[\text{SO}_2]^{0.6} \cdot Rh_{60} \cdot e^{f(T)} + 0.593\text{PM}_{10} + 1.29\text{Rain} \cdot [H^+] \quad (1)$$

$$f(T) = 0.15(T - 10), \text{ for } T < 10\text{ }^\circ\text{C} \quad (1a)$$

$$f(T) = -0.054(T - 10), \text{ for } T \geq 10\text{ }^\circ\text{C} \quad (1b)$$

Zinc

$$ML = 3.5 + 0.471[\text{SO}_2]^{0.22} \cdot e^{0.018Rh + f(T)} + 1.37[\text{HNO}_3] + 0.041\text{Rain} [H^+] \quad (2)$$

$$f(T) = 0.062(T - 10), \text{ for } T < 10\text{ }^\circ\text{C} \quad (2a)$$

$$f(T) = -0.021(T - 10), \text{ for } T \geq 10\text{ }^\circ\text{C} \quad (2b)$$

Limestone

$$R = 4 + 0.0059[SO_2] \cdot Rh_{60} + 0.078[HNO_3] \cdot Rh_{60} + 0.0258PM_{10} + 0.054Rain[H^+] \quad (3)$$

Modern glass

$$H = (0.2215[SO_2] + 0.1367[NO_2] + 0.1092PM_{10}) / (1 + (382/t)^{1.86}) \quad (4)$$

where

ML = mass loss (the difference in the specimen's initial mass minus the remaining mass after removing its corroded part), g m⁻²;

R = surface recession, μm (absolute values);

H = haze, %;

t = exposure time, in days;

Rh = relative humidity, %—annual average;

Rh₆₀ = Rh − 60 when Rh > 60, 0 otherwise;

T = mean annual temperature, °C;

[SO₂] = mean annual concentration, μg m⁻³;

[NO₂] = mean annual concentration, μg m⁻³;

[HNO₃] = mean annual concentration, μg m⁻³;

Rain = precipitation amount, mm year⁻¹—total rain amount in one year;

PM₁₀ = mean annual concentration, μg m⁻³;

[H⁺] = mean annual concentration, mg L⁻¹. The unit for [H⁺] is not the normal one (mol L⁻¹) used for this denomination and the relationship between pH and [H⁺] is therefore [H⁺] = 1007.97 × 10^{-pH} ≈ 10^{3-pH} here.

In the case of [HNO₃], if in situ measurements are unavailable, then the concentration is estimated by Equation (5) [22].

$$[HNO_3] = 516 \cdot e^{-3400/(T+273)} \cdot ([NO_2][O_3]Rh)^{0.5} \quad (5)$$

where

[O₃] = mean annual concentration, μg m⁻³.

In the above DRFs, and all other available DRFs in the literature, it is clearly shown that they rely solely on the availability of ground-based data to provide deterioration estimates of the different materials. This is a major limitation of the utility of these models because, among other things, it is difficult and expensive to deploy the necessary network of ground-based stations at all sites of interest. The authors believe that the solution to this may be the development of SSD-DRFs. Nowadays, the multitude of different satellite data enables us to develop new techniques and approaches.

2.2. Satellite Remote Sensing Data

Satellite air quality data from the Ozone Monitoring Instrument (OMI), the Atmospheric Infrared Sounder (AIRS) and the Moderate Resolution Imaging Spectroradiometer (MODIS) were used for this purpose. Specifically, concentration data for O₃, NO₂ and SO₂ were collected by OMI [29–31], air temperature (Temp) data were collected by AIRS [32] and Aerosol Optical Depth (AOD) data were collected by MODIS [33]. In the case of relative humidity (RH), reanalysis data from the European Centre for Medium-Range Weather Forecasts (ECMWF) were used. This fact was deemed necessary since satellite-derived relative humidity data show little correlation with ground-based data.

Data were collected for the same time periods and sites as the ICP Materials exposure campaigns. Table 1 shows the time periods of the exposure campaigns, and all the cities where the campaigns took place are shown in Table 2.

Table 1. Time periods of ICP Materials exposure campaigns.

Exposure Campaign	Time Period
Exposure 1	2005–2006 [34]
Exposure 2	2008–2009 [35]
Exposure 3	2011–2012 [36]
Exposure 4	2014–2015 [37]
Exposure 5	2017–2018 [38]

Table 2. ICP Materials exposure sites for time periods (2005–2006, 2008–2009, 2011–2012, 2014–2015, 2017–2018) [34–38].

Exposure Site	Exposure Period	Exposure Site	Exposure Period
Aspvreten	1, 2, 3, 4, 5	Paris	1, 2, 3, 4, 5
Athens	1, 2, 3, 4, 5	Prague	1, 2, 3, 4, 5
Berlin	1, 2, 3, 4, 5	Riga	1, 2, 3, 4
Birkenes	1, 2, 3, 4, 5	Rome	1, 2, 3, 4, 5
Bottrop	1, 2, 3, 4, 5	Sofia	2
Casaccia	1, 2, 3, 4, 5	Split	5
Chaumont	1, 2, 3, 4, 5	St. Petersburg	3
Hameenlinna	4, 5	Stockholm	1, 2, 3, 4, 5
Katowice	1, 2, 3, 4, 5	Svanvik	1, 2, 3, 4, 5
Kopisty	1, 2, 3, 4, 5	Toledo	1, 2, 3, 4, 5
Lahemaa	1, 2, 4	Venice	1, 2, 3, 4, 5
Madrid	1, 2, 3, 4, 5	Vienna	2, 3, 4, 5
Milan	1, 2, 3, 4, 5	Zagreb	5
Oslo	1, 2, 3, 4, 5	Zilina	4, 5

In addition to satellite and reanalysis data, corrosion/soiling results from the above-mentioned exposure campaigns were collected for the needs of the SSD-DRFs being developed. The corrosion/soiling results were used to develop and test the new SSD-DRFs [39–46].

3. Results

Multiple regression analysis, a supervised machine learning technique, was performed to develop the SSD-DRFs. Due to the non-linearity of the corrosion/soiling effect, and the complexity that presents such problems from a study point of view, an attempt was made to convert the non-linear problem into a linear one. As mentioned earlier, the corrosion/soiling effect is a multi-factorial effect. If we consider that observed deterioration results from the synergistic effect of all meteorological and air pollution parameters, we can consider that the non-linear Equation (6) describes the relationship between them.

$$D = [X_1]^A \cdot [X_2]^B \cdot \dots \cdot [X_n]^N \quad (6)$$

where

D = deterioration;

$[X_i]^j$ = corrosion/soiling parameters, where i denotes different parameters or products of parameters and j denotes the exponent of the i term.

If we calculate the logarithm of Equation (6), then the following relationship is obtained:

$$\ln(D) = A \cdot \ln([X_1]) + B \cdot \ln([X_2]) + \dots + N \cdot \ln([X_n]) \quad (7)$$

When trying to model the response using a single predictor or more variables, Pearson's correlation is used to estimate a linear correlation coefficient between the predictors and the target. In our case, the meteorological parameters and air pollutants mentioned above are the predictive factors and the target is the corrosion/soiling of the material. One of the first sources of non-linearity is due to different interactions between predictors. For

instance, the synergistic effects on corrosion between NO₂, O₃ and SO₂, combined with the relative humidity, affect the amount and form of water available on a material's surface. To examine the linear relationship of the interaction between parameters and corrosion, the interaction terms must be multiplied by themselves.

In addition, in this study, an attempt was made to insert SSD-DRFs, a term for pollutants' diffusivity, on the material surfaces, as it is known that atmospheric corrosion can occur either in a dry environment (low humidity) or in a wet environment (high humidity). In the case of high humidity, a thin film of water forms on the material's surface (Figure 1). Air pollutants can diffuse into this water film, resulting in an acceleration of the corrosion effect [47]. This mechanism is modelled in the SSD-DRFs by incorporating the diffusion coefficient parameter into them.

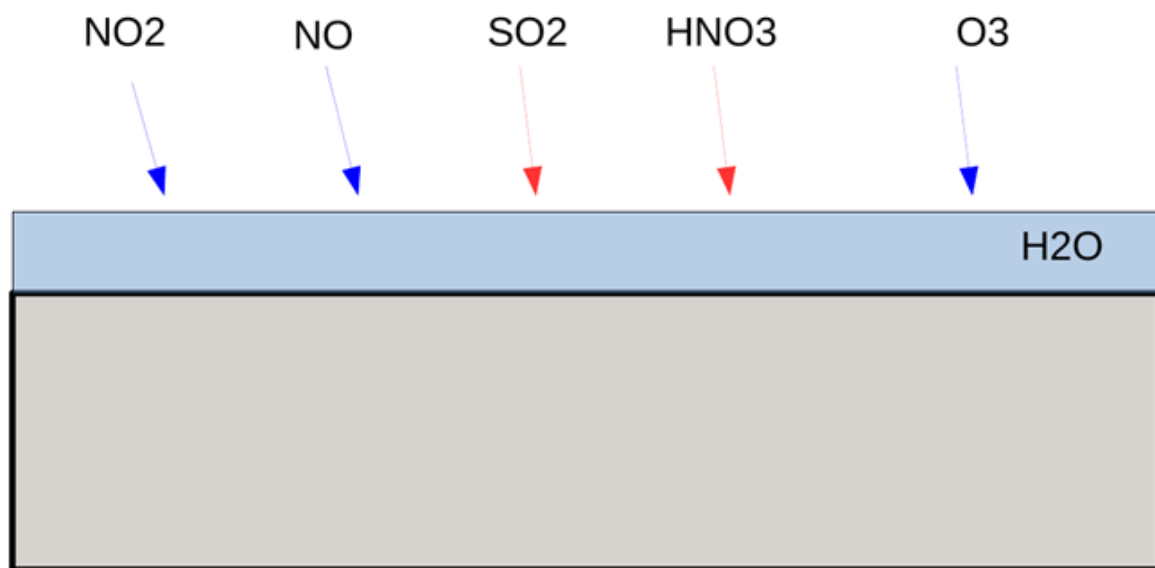


Figure 1. Thin film of water formation on the material's surface.

As has been shown, the diffusion coefficient, D , in a single diffusion mode obeys an Arrhenius-like behavior, as seen in Equation (8):

$$D = D_0 \cdot \exp \left[\frac{-E}{(K_B T)} \right] \quad (8)$$

where the activation energy E and the pre-exponential factor D_0 are essentially temperature independent, and K_B is the Boltzmann constant. From Equation (8), it is possible to calculate the values of the activation energy E through the slope of the plot of $\ln D$ vs. $1/T$ [48]. In the following years, many experimental studies were carried out using infrared laser resonant desorption (LRD) techniques to calculate diffusion coefficients in ice film [49–55]. The results from these studies confirmed the linear relationship between $\ln D$ and $1/T$ [56]. This result clearly suggests that Equation (8) can be used to estimate the diffusion coefficient at any temperature when the diffusion coefficient at two different temperatures is known.

Varotsos and Zellner [56] used the above studies [53,54] and found a significant result, namely that there is a linear relationship between the natural logarithm of the pre-exponential factor D_0 and the activation energy E (i.e., $\ln D_0$ vs. E). Summarizing all the above studies, it is concluded that it is possible to estimate the diffusion coefficients of other important species in ice. Based on the same theory, it is possible to calculate the diffusion coefficient of any important species we want in the thin film of water on the material's surface. Thus, if the diffusion coefficient is known at two different temperatures, from the slope of the $\ln D$ vs. $1/T$ plot, it is possible to calculate the diffusion coefficient at any temperature. The diffusion coefficients of O₃ [57], NO₂ [58] and SO₂ [59] in water, at different temperatures, are available from laboratory experiments that are presented

in the literature. The resulting equations for the diffusion coefficients are the following (Equations (9)–(11)):

$$D_{O_3} = 1.1 \times 10^{-6} \exp\left(\frac{-1896}{T}\right) \quad (9)$$

$$D_{NO_2} = \exp\left[(-1.885) \cdot \left(\frac{1000}{T}\right) + 6.641\right] \quad (10)$$

$$D_{SO_2} = \exp\left[(-2.96) \cdot \left(\frac{1000}{T}\right) + 10.42\right] \quad (11)$$

The resulting diffusion coefficients from Equations (9)–(11) for each site in the exposure campaigns were multiplied by the corresponding atmospheric pollutant concentration, as derived from satellite data. After multiplications between all parameters, 36 products were calculated. These products were used to investigate the correlation of each of them with the corrosion/soiling experimental results of each material by calculating the Pearson's correlation coefficient. According to the obtained results, different parameters showed a linear correlation with the corrosion/soiling in each material. The parameters that correlate well with the corrosion/soiling of each material have been used in SSD-DRFs development.

Tables 3–6 present the results of Pearson's correlation coefficient calculations between environmental parameters and corrosion/soiling estimates. For the case of carbon steel, Table 3, it is evident that this material presents the highest correlation coefficients with relative humidity (RH), parameters, the product of RH with NO₂ and AOD (Aerosol Optical Depth) concentrations, as well as the product of RH², NO₂ and SO₂ concentrations. The asterisks denote the statistical significance level of the obtained correlation coefficients. The parameter N in the following tables denotes the number of samples of experimental corrosion/soiling values used in each case.

Table 3. Chosen parameters for carbon steel mass loss SSD-DRF.

		RH	RH * NO ₂	RH * AOD	RH ² * NO ₂ * SO ₂
Mass loss	Pearson Correlation	0.498 **	0.443 **	0.611 **	0.484 **
	N	110	110	110	110

** Correlation is significant at the 0.01 level (2-tailed).

Table 4. Chosen parameters for zinc mass loss SSD-DRF.

		RH	RH * O ₃	RH * SO ₂
Mass loss	Pearson Correlation	0.383 **	0.386 **	0.232 *
	N	112	112	112

** Correlation is significant at the 0.01 level (2-tailed). * Correlation is significant at the 0.05 level (2-tailed).

Table 5. Chosen parameters for limestone mass loss SSD-DRF.

		RH	RH * NO ₂	RH * AOD
Mass loss	Pearson Correlation	0.234 *	0.202 *	0.127
	N	105	105	105

* Correlation is significant at the 0.05 level (2-tailed).

Table 6. Chosen parameters for modern glass soiling SSD-DRF.

		Temp	AOD	SO ₂ * D _{SO2}	NO ₂ * D _{NO2}	O ₃ * D _{O3}
Soiling	Pearson Correlation	0.612 **	0.465 **	0.434 **	0.360 **	0.586 **
	N	97	97	97	97	97

** Correlation is significant at the 0.01 level (2-tailed).

For the case of zinc (Table 4), it is evident that this material presents the highest correlation coefficients with the parameters of RH and the product of RH with the concentrations of O₃ and SO₂.

For the case of limestone (Table 5), it is obvious that this material, in all cases, presents low values of correlation coefficients; however, we have considered the highest of them, i.e., RH and the product of RH with O₃ concentration. Both are statistically significant at the 0.05 level. Analyzing the obtained results, it was evident that these two parameters could not adequately model the limestone's corrosion, so it was decided that the product of RH with SO₂ concentration should also be used, which, according to the literature [4], is an air pollutant that affects limestone's corrosion.

For the case of modern glass (Table 6), it was found that this material presents the highest correlation coefficients with the climatic parameter of temperature (Temp), the air quality parameter of AOD and the products of the SO₂, NO₂ and O₃ concentrations with their diffusion coefficients, respectively.

After selecting the parameters to be used to develop SSD-DRFs, linear regression analysis was applied using the Sklearn library in python. To apply this tool, the entire data set was split into train and test sets in a ratio of 80–20% and with the help of a loop we run regression analysis 10,000 times for each material. Each run resulted in 10,000 different sets of constants and coefficients for the parameters. In the next step, we kept only the results where all parameters were positive, because a negative parameter would mean a decrease in corrosion with increasing pollutant concentration, which is contrary to current knowledge. In the end, from the remaining results, we selected the set of a coefficient and constant value which showed similar accuracy in train/test sets and the whole data set.

The following list gives the mathematical formulation of the SSD-DRF of each material (Equations (12)–(15)):

Carbon steel

$$ML = 2.389 \cdot \ln(RH) + 0.332 \cdot \ln(RH \cdot NO_2) + 1.313 \cdot \ln(RH \cdot AOD) + 0.007 \cdot \ln(RH^2 \cdot SO_2 \cdot NO_2) - 23.988 \quad (12)$$

Zinc

$$ML = 0.32 \cdot \ln(RH) + 0.921 \cdot \ln(RH \cdot O_3) + 0.00035 \cdot \ln(RH \cdot SO_2) \quad (13)$$

Limestone

$$R = 0.433 \cdot \ln(RH) + 0.18 \cdot \ln(RH \cdot O_3) + 0.095 \cdot \ln(RH \cdot SO_2) - 1.914 \quad (14)$$

Modern glass

$$H = 16.511 \cdot \ln(Temp) + 0.824 \cdot \ln(AOD) + 0.018 \cdot \ln(NO_2 \cdot D_{NO2}) + 0.333 \cdot \ln(O_3 \cdot D_{O3}) + 0.015 \cdot \ln(SO_2 \cdot D_{SO2}) - 94.12 \quad (15)$$

These functions were then used to calculate the corrosion/soiling estimates of the different materials at each different site during all exposure periods. Table 7 gives the Pearson's correlation coefficient obtained by investigating the linear correlation between the SSD-DRFs corrosion/soiling estimates and the experimental data. The size of the paired samples used for each material is given in the second line of Table 7.

Table 7. Pearson correlation coefficients between SSD-DRFs estimates and experimental data.

	Carbon Steel (Observed Mass Loss)	Zinc (Observed Mass Loss)	Limestone (Observed Recession)	Modern Glass (Observed Soiling)
SSD-DRF	0.613 **	0.367 **	0.240 **	0.633 **
N	110	112	105	97

** Correlation is significant at the 0.01 level (2-tailed).

Table 8 shows the Pearson's correlation coefficients between G-DRFs and experimental data as well as SSD-DRFs and experimental data, where the name G-DRFs refers to the existing DRFs, Equations (1)–(4), which use ground-based data as inputs. The size of the paired samples used for each material is given in the third line of Table 8.

Table 8. Pearson correlation coefficients between G-DRFs and experimental data, SSD-DRFs and experimental data.

	Carbon Steel (Observed Mass Loss)	Zinc (Observed Mass Loss)	Limestone (Observed Recession)	Modern Glass (Observed Soiling)
G-DRF	0.511 **	0.207 *	0.327 *	0.413 **
SSD-DRF	0.589 **	0.364 **	0.401 **	0.723 **
N	55	73	55	71

** Correlation is significant at the 0.01 level (2-tailed). * Correlation is significant at the 0.05 level (2-tailed).

Figures 2–5 show the observed experimentally (OBS) corrosion/soiling values estimated using SSD-DRFs (SSD-DRFs) and estimated using G-DRFs (G-DRF) for the case of carbon steel, zinc, limestone and modern glass, respectively, at the indicated sites.

Figure 6 presents, in the form of box plots, the statistics of the relative differences between SSD-DRFs and G-DRF estimates in experimentally obtained corrosion/soiling values.

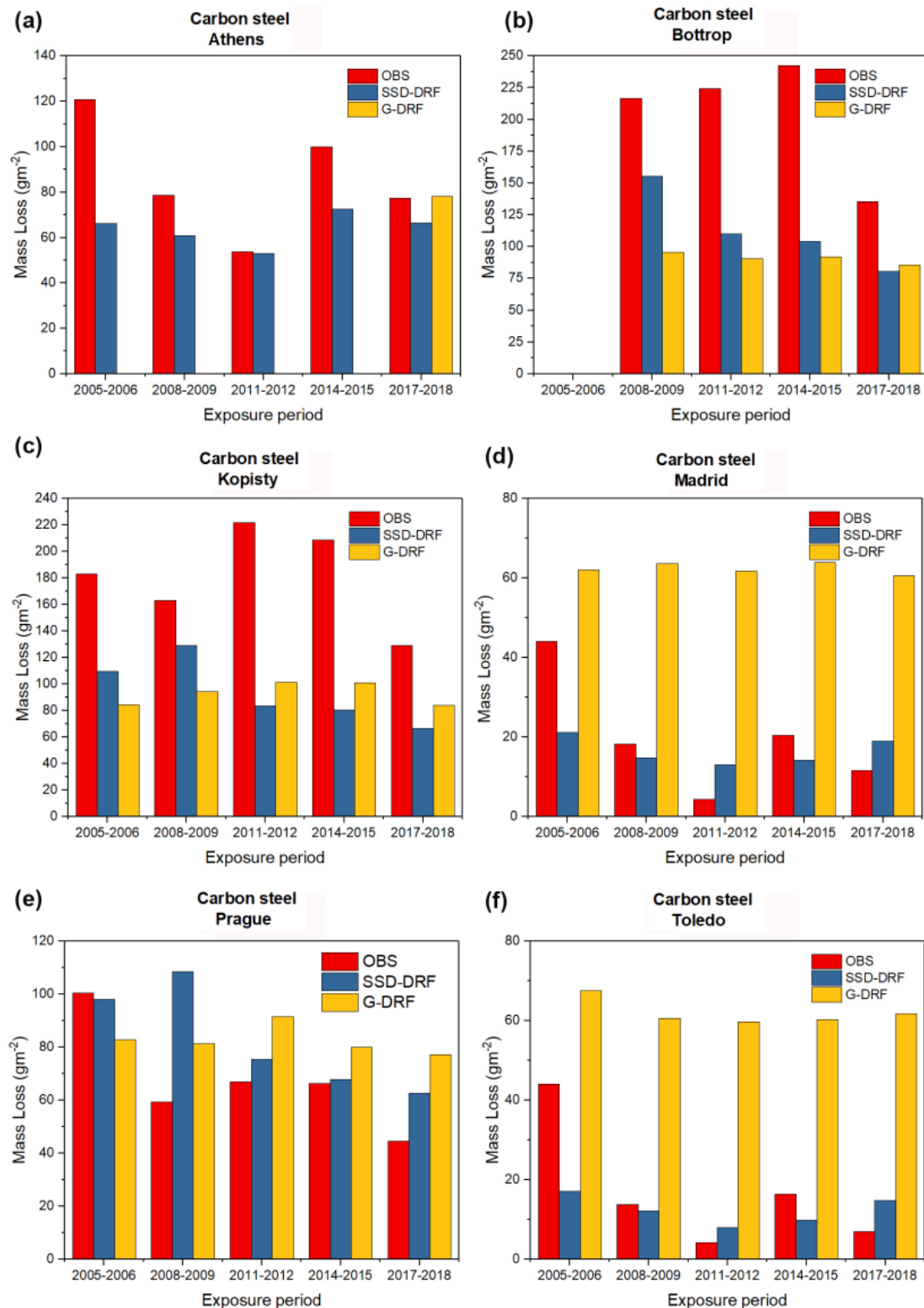


Figure 2. The experimentally observed mass loss of carbon steel (red bars), the estimated mass loss of carbon steel using SSD-DRF (blue bars) and the estimated mass loss of carbon steel using G-DRF (yellow bars) for case (a) Athens, (b) Bottrop, (c) Kopisty, (d) Madrid, (e) Prague and (f) Toledo after five different one-year exposure periods (2005–2006, 2008–2009, 2011–2012, 2014–2015, 2017–2018). The missing yellow bars in the case of Athens are due to the lack of the necessary ground-based data necessary for the application of G-DRF.

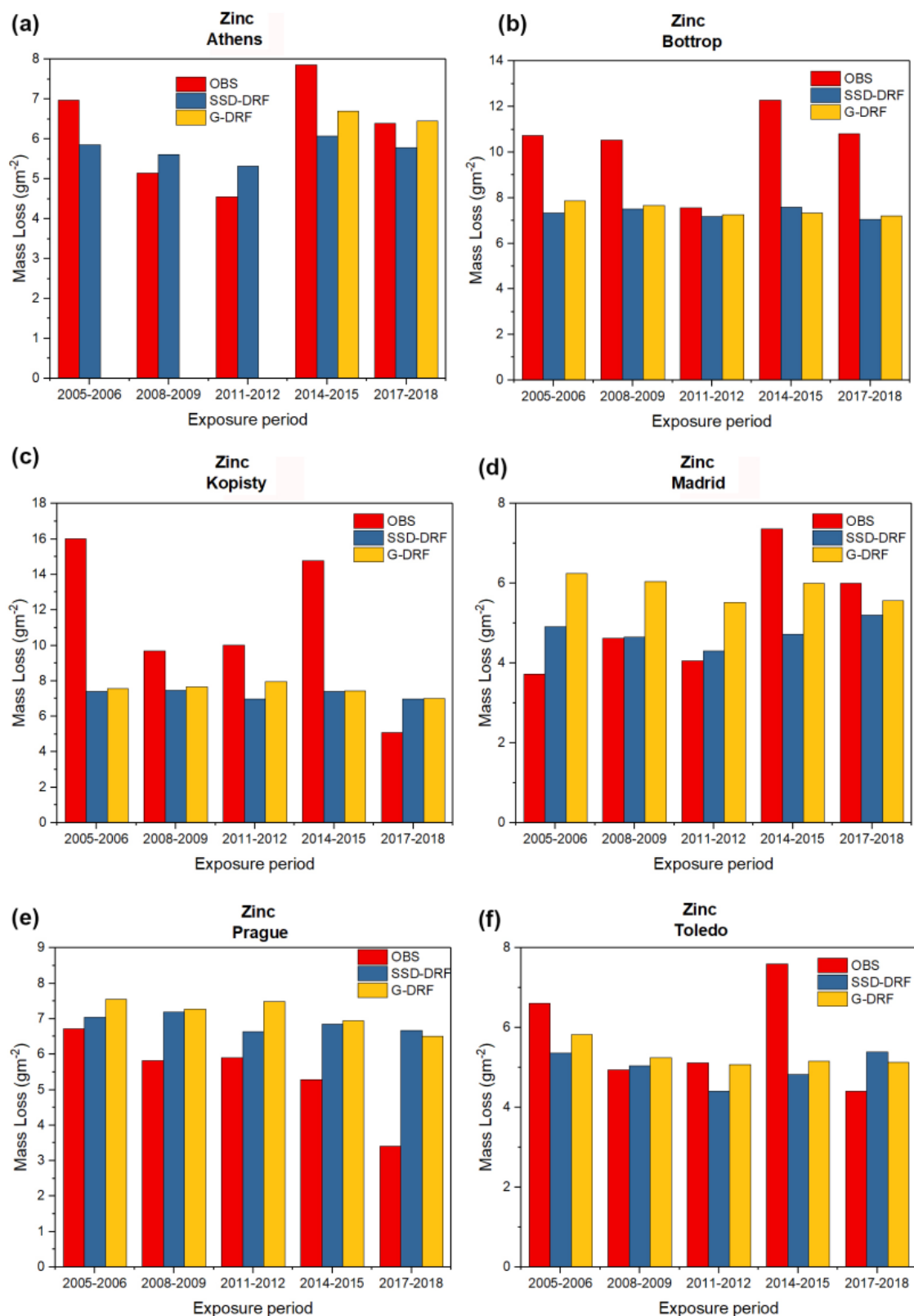


Figure 3. As in Figure 2, but for the case of zinc. (a) Athens, (b) Bottrop, (c) Kopisty, (d) Madrid, (e) Prague and (f) Toledo.

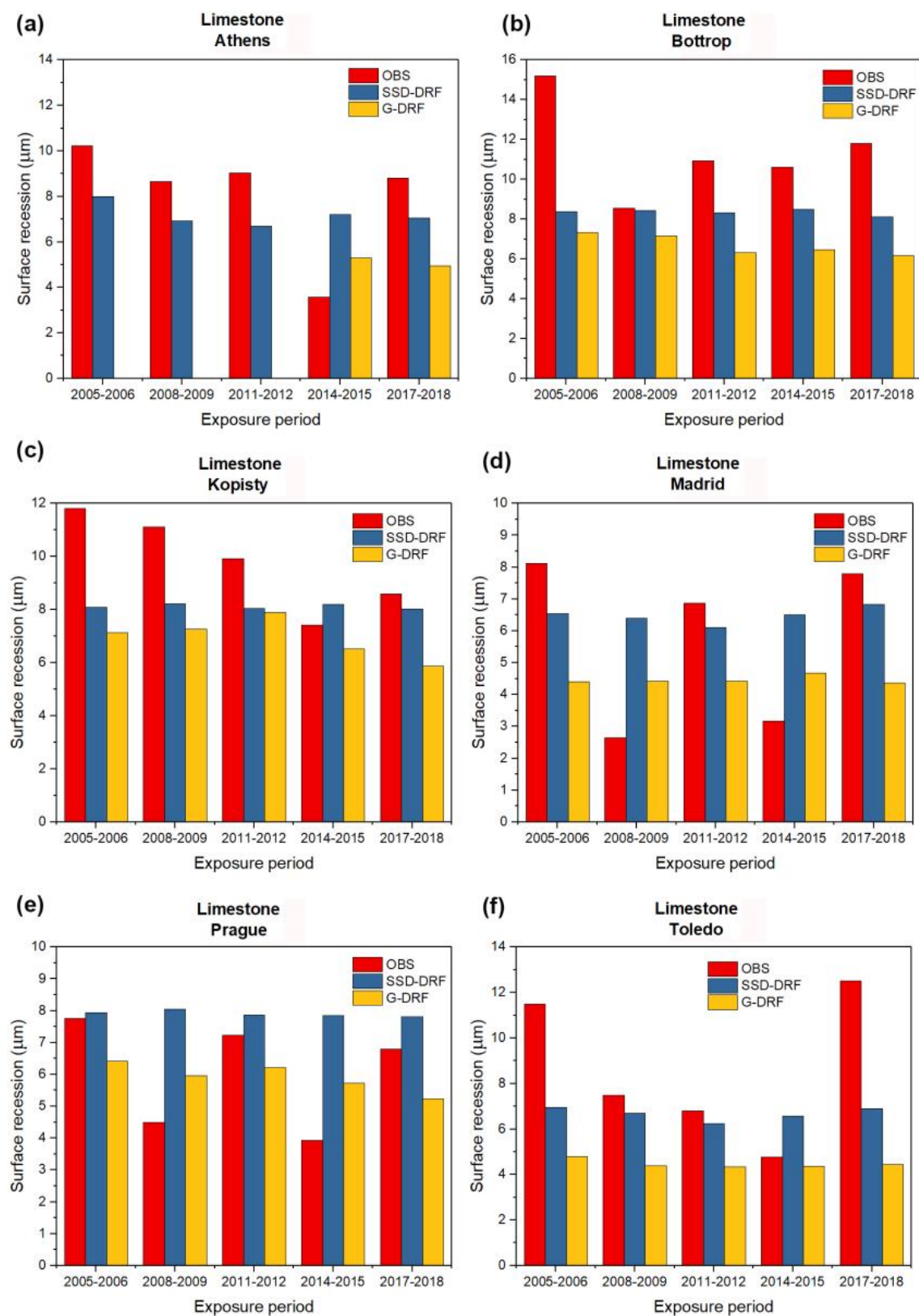


Figure 4. As in Figure 2, but for the case of Limestone. (a) Athens, (b) Bottrop, (c) Kopisty, (d) Madrid, (e) Prague and (f) Toledo.

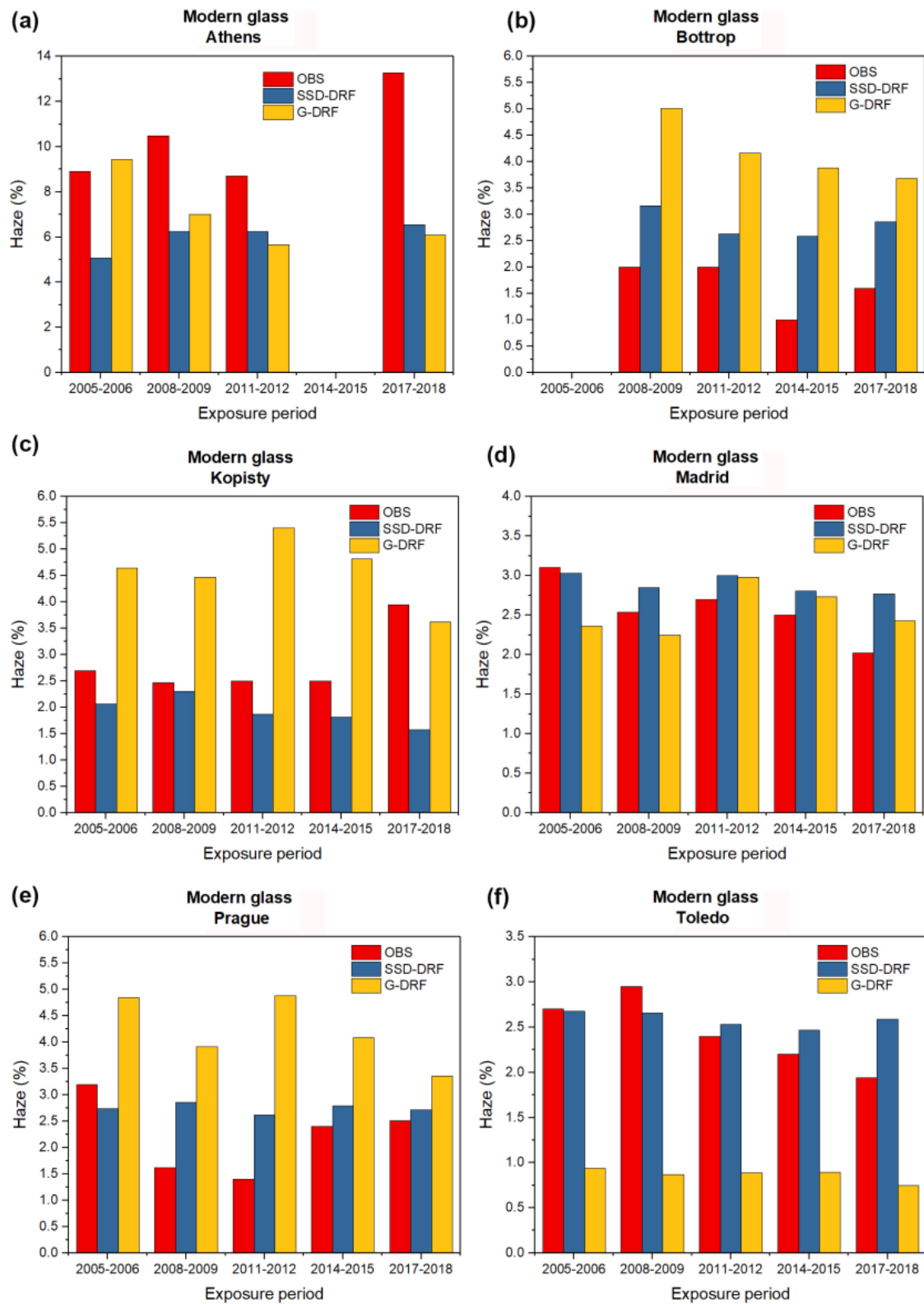


Figure 5. As in Figure 2, but for the case of modern glass haze. (a) Athens, (b) Bottrop, (c) Kopisty, (d) Madrid, (e) Prague and (f) Toledo. The gaps at Athens and Bottrop at the exposure periods of 2005–2006 and 2008–2009, respectively, are due to a lack of experimental data.

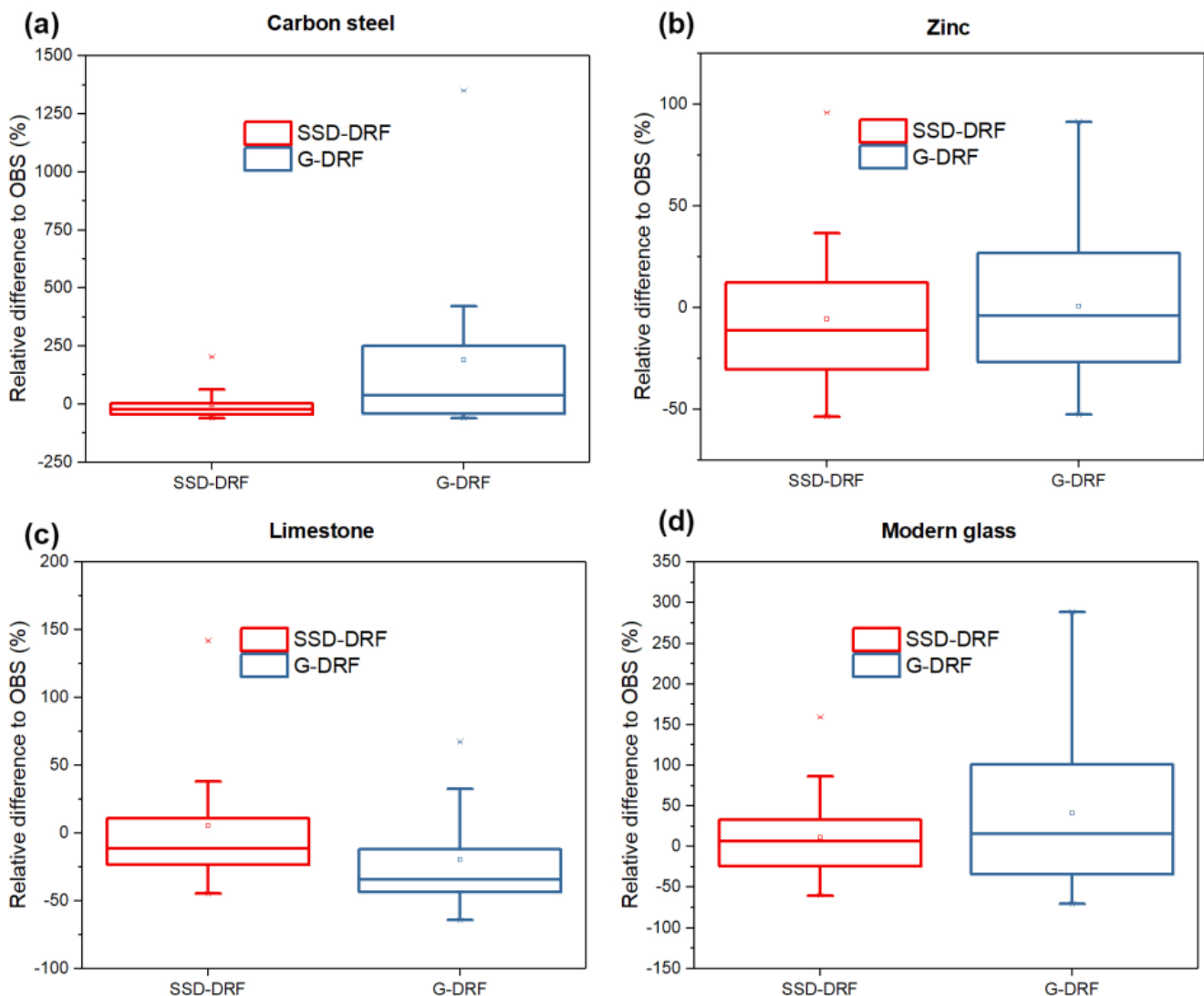


Figure 6. The relative differences between corrosion/soiling estimates calculated using SSD-DRFs and G-DRFs and experimentally obtained data for the case of (a) carbon steel mass loss, (b) zinc mass loss, (c) limestone recession and (d) modern glass haze.

4. Discussion and Conclusions

According to Table 8, the corrosion/soiling estimates produced by SSD-DRFs show a better correlation with the experimental results than the estimates produced by G-DRFs for all materials studied. This means that the SSD-DRFs developed using only satellite data improve the corrosion/soiling estimation results compared to the already available G-DRFs, which use only ground-based data. This conclusion is also supported by the box plots presented in Figure 6. According to these results, the populations with relative differences between the corrosion/soiling estimates, calculated using SSD-DRFs, and experimentally obtained data have a smaller range, excluding the extreme values, and in most cases their medians are closer to zero than the same results estimated using G-DRFs.

Another remark is related to data availability. According to Table 7, the sizes of the available sample pairs of carbon steel, zinc, limestone and modern glass are 110, 112, 105 and 97, respectively. As for G-DRFs, their usability is limited by the availability of ground-based data. Due to the lack of necessary data, the sizes of the available sample pairs given in Table 8 are 55, 73, 55 and 71 for carbon steel, zinc, limestone and modern glass, respectively. This means that the applicability of SSD-DRFs increases for the various

materials by about 200%, 150%, 190% and 135%, respectively. This is confirmed by the graphs plotted in Figures 2–4 for the case of Athens. Yellow bars indicating G-DRFs estimates of carbon steel, zinc and limestone corrosion are missing for the exposure periods 2005–2006, 2008–2009 and 2011–2012 (and 2014–2015 carbon steel only) due to a lack of some necessary ground-based data. In contrast, the availability of satellite data meets the data needs of SSD-DRFs to enable continuous monitoring of the corrosion/soiling.

It should be mentioned that satellite data also offer an almost global coverage, which means that the proposed SSD-DRFs can be directly applied to almost any part of the globe according to user needs (e.g., cultural heritage managers, stakeholders, policy makers, etc.). In addition, this new tool offers the potential to produce continuous large-scale corrosion/soiling mapping, without the need for ground-based meteorological and pollution networks. Thus, the SSD-DRFs tool could act as a global corrosion/soiling monitoring system capable of identifying “hot spots” across the planet and/or providing warnings about sensitive areas at an early stage, offering valuable time to address any type of problematic status.

Although we have historical air pollution data, more work needs to be carried out to improve the knowledge and accuracy of corrosion/soiling estimation obtained with satellite data to contribute, inter alia, to the achievement of the Sustainable Development Goals—UN 2030 Agenda [60,61].

Author Contributions: Conceptualization, J.C. and G.K.; methodology, J.C. and G.K.; software, G.K.; validation, G.K., Y.X. and J.C.; formal analysis, G.K.; investigation, G.K.; data curation, G.K. and Y.X.; writing—original draft preparation, G.K. and J.C.; writing—review and editing, Y.X. and C.V.; supervision, C.V.; project administration, C.V. All authors have read and agreed to the published version of the manuscript.

Funding: This research received no external funding.

Data Availability Statement: Publicly available datasets were analyzed in this study. This data can be found here: <https://www.ri.se/en/icp-materials/documents/icp-materials-reports>.

Acknowledgments: A large part of this research was carried out in the frame of the Dragon Project “Air quality over China” and ICP Materials.

Conflicts of Interest: The authors declare no conflict of interest.

References

1. Bhaskaran, R.; Palaniswamy, N.; Rengaswamy, N.; Jayachandran, M. Global Cost of Corrosion—A Historical Review. In *ASM Handbook Volume 13B, Corrosion: Materials*; ASM International: Detroit, MI, USA, 2005; Volume 13, p. 704. ISBN 978-0-87170-707-9.
2. Ebel, A.; Davitashvili, T. *Air, Water and Soil Quality Modelling for Risk and Impact Assessment*; NATO Security through Science Series C; Springer: Dordrecht, The Netherlands, 2007; ISBN 978-1-4020-5875-2.
3. Varotsos, C.; Tzanis, C.; Cracknell, A. The Enhanced Deterioration of the Cultural Heritage Monuments Due to Air Pollution. *Environ. Sci. Pollut. Res.* **2009**, *16*, 590–592. [[CrossRef](#)] [[PubMed](#)]
4. Tidblad, J.; Kucera, V.; Ferm, M.; Kreislova, K.; Brüggerhoff, S.; Doytchinov, S.; Screpanti, A.; Grøntoft, T.; Yates, T.; De La Fuente, D.; et al. Effects of Air Pollution on Materials and Cultural Heritage: ICP Materials Celebrates 25 Years of Research. *Int. J. Corros.* **2012**, *2012*, 496321. [[CrossRef](#)]
5. Tzanis, C.; Varotsos, C.; Ferm, M.; Christodoulakis, J.; Assimakopoulos, M.N.; Efthymiou, C. Nitric Acid and Particulate Matter Measurements at Athens, Greece, in Connection with Corrosion Studies. *Atmos. Chem. Phys.* **2009**, *9*, 8309–8316. [[CrossRef](#)]
6. Tzanis, C.; Varotsos, C.; Christodoulakis, J.; Tidblad, J.; Ferm, M.; Ionescu, A.; Lefevre, R.-A.; Theodorakopoulou, K.; Kreislova, K. On the Corrosion and Soiling Effects on Materials by Air Pollution in Athens, Greece. *Atmos. Chem. Phys.* **2011**, *11*, 12039–12048. [[CrossRef](#)]
7. Hudson, J.C.; Stanners, J.F. The Effect of Climate and Atmospheric Pollution on Corrosion. *J. Appl. Chem.* **2007**, *3*, 86–96. [[CrossRef](#)]
8. Vernon, W.H.J. A Laboratory Study of the Atmospheric Corrosion of Metals. Part I.—The Corrosion of Copper in Certain Synthetic Atmospheres, with Particular Reference to the Influence of Sulphur Dioxide in Air of Various Relative Humidities. *Trans. Faraday Soc.* **1931**, *27*, 255–277. [[CrossRef](#)]
9. Vernon, W.H.J. A Laboratory Study of the Atmospheric Corrosion of Metals. Part II.—Iron: The Primary Oxide Film. Part III.—The Secondary Product or Rust (Influence of Sulphur Dioxide, Carbon Dioxide, and Suspended Particles on the Rusting of Iron). *Trans. Faraday Soc.* **1935**, *31*, 1668–1700. [[CrossRef](#)]

10. Johansson, L.-G. Synergistic Effects of Air Pollutants on the Atmospheric Corrosion of Metals and Calcareous Stones. *Mar. Chem.* **1990**, *30*, 113–122. [\[CrossRef\]](#)
11. Eriksson, P.; Johansson, L.-G.; Strandberg, H. Initial Stages of Copper Corrosion in Humid Air Containing SO₂ and NO₂. *J. Electrochem. Soc.* **1993**, *140*, 53–59. [\[CrossRef\]](#)
12. Zakipour, S.; Tidblad, J.; Leygraf, C. Atmospheric Corrosion Effects of SO₂ and O₃ on Laboratory-Exposed Copper. *J. Electrochem. Soc.* **1995**, *142*, 757. [\[CrossRef\]](#)
13. Strandberg, H.; Johansson, L. Role of O₃ in the Atmospheric Corrosion of Copper in the Presence of SO₂. *J. Electrochem. Soc.* **1997**, *144*, 2334. [\[CrossRef\]](#)
14. Feliu, S.; Mariaca, L.; Simancas, J.; González, J.A.; Morcillo, M. Effect of NO₂ and/or SO₂ Atmospheric Contaminants and Relative Humidity on Copper Corrosion. *Rev. Metal.* **2003**, *39*, 279–288. [\[CrossRef\]](#)
15. Mariaca, L.; de la Fuente, D.; Feliu, S.; Simancas, J.; González, J.A.; Morcillo, M. Interaction of Copper and NO₂: Effect of Joint Presence of SO₂, Relative Humidity and Temperature. *J. Phys. Chem. Solids* **2008**, *69*, 895–904. [\[CrossRef\]](#)
16. Svensson, J.-E.; Johansson, L.-G. A Laboratory Study of the Effect of Ozone, Nitrogen Dioxide, and Sulfur Dioxide on the Atmospheric Corrosion of Zinc. *J. Electrochem. Soc.* **1993**, *140*, 2210. [\[CrossRef\]](#)
17. Castaño, J.G.; de la Fuente, D.; Morcillo, M. A Laboratory Study of the Effect of NO₂ on the Atmospheric Corrosion of Zinc. *Atmos. Environ.* **2007**, *41*, 8681–8696. [\[CrossRef\]](#)
18. Allen, G.C.; El-Turki, A.; Hallam, K.R.; McLaughlin, D.; Stacey, M. Role of NO₂ and SO₂ in Degradation of Limestone. *Br. Corros. J.* **2000**, *35*, 35–38. [\[CrossRef\]](#)
19. Mangio, R.; Johansson, L. The Influence of Ozone on the Atmospheric Corrosion of Carrara Marble in Humid Atmospheres Containing Sulfur Dioxide, Deposition Studies of SO₂ on Marble. In Proceedings of the 11th Scandinavian Corrosion Congress, Stavanger, Norway, 1–6 October 1989.
20. Ferm, M.; De Santis, F.; Varotsos, C. Nitric Acid Measurements in Connection with Corrosion Studies. *Atmos. Environ.* **2005**, *39*, 6664–6672. [\[CrossRef\]](#)
21. Ferm, M.; Watt, J.; O'Hanlon, S.; De Santis, F.; Varotsos, C. Deposition Measurement of Particulate Matter in Connection with Corrosion Studies. *Anal. Bioanal. Chem.* **2006**, *384*, 1320–1330. [\[CrossRef\]](#)
22. Kucera, V.; Tidblad, J.; Samie, F.; Schreiner, M.; Melcher, M.; Kreislova, K.; Lefevre, R.-A.; Ionescu, A.; Snethlage, R.; Varotsos, C.; et al. *Model for Multi-Pollutant Impact and Assessment of Threshold Levels for Cultural Heritage Publishable Final Report*; Swedish Corrosion Institute (SCI): Stockholm, Sweden, 2005; p. 52.
23. Kucera, V.; Tidblad, J.; Kreislova, K.; Knotkova, D.; Faller, M.; Reiss, D.; Snethlage, R.; Yates, T.; Henriksen, J.; Schreiner, M.; et al. UN/ECE ICP Materials Dose-Response Functions for the Multi-Pollutant Situation. *Water Air Soil Pollut. Focus* **2007**, *7*, 249–258. [\[CrossRef\]](#)
24. Gil, H.; Buitrago, C.P.; Calderón, J.A. Atmospheric Corrosion of Copper and Silver Influenced by Particulate Matter. *J. Solid State Electrochem.* **2017**, *21*, 1111–1119. [\[CrossRef\]](#)
25. Samie, F.; Tidblad, J.; Kucera, V.; Leygraf, C. Atmospheric Corrosion Effects of HNO₃: A Comparison of Laboratory and Field Exposed Copper, Zinc, and Carbon Steel. *J. Electrochem. Soc.* **2007**, *154*, C249. [\[CrossRef\]](#)
26. Samie, F.; Tidblad, J.; Kučera, V.; Leygraf, C. Atmospheric Corrosion Effects of HNO₃—Influence of Temperature and Relative Humidity on Laboratory-Exposed Copper. *Atmos. Environ.* **2007**, *41*, 1374–1382. [\[CrossRef\]](#)
27. Samie, F.; Tidblad, J. Influence of Nitric Acid on Atmospheric Corrosion of Copper, Zinc and Carbon Steels. *Corros. Eng. Sci. Technol.* **2008**, *43*, 117–122. [\[CrossRef\]](#)
28. Verney-Carron, A.; Lombardo, T. *UN/ECE International Cooperative Programme on Effects on Materials, Including Historic and Cultural Monuments, Report No 74: Results of the Exposure of Modern Glass 2008–2012 and Soiling Dose-Response Functions*; Laboratoire Interuniversitaire des Systèmes Atmosphérique (LISA): Paris, France, 2013.
29. Bhartia, P.K. *OMI/Aura TOMS-Like Ozone and Radiative Cloud Fraction L3 1 Day 0.25 Degree x 0.25 Degree V3*; NASA Goddard Space Flight Center, Goddard Earth Sciences Data and Information Services Center: Greenbelt, MD, USA, 2012.
30. Krotkov, N.A.; Lamsal, L.N.; Marchenko, S.V.; Celarier, E.A.; Bucsela, E.J.; Swartz, W.H.; Joiner, J. *The OMI Core Team OMI/Aura NO₂ Cloud-Screened Total and Tropospheric Column L3 Global Gridded 0.25 Degree x 0.25 Degree V3*; NASA Goddard Space Flight Center, Goddard Earth Sciences Data and Information Services Center: Greenbelt, MD, USA, 2019.
31. Li, J.; Yang, H.; Liu, X.; Yu, N.; Tian, Y.; Zhou, X.; Zhang, P.; Wang, K. Aircraft Emission Inventory and Characteristics of the Airport Cluster in the Guangdong–Hong Kong–Macao Greater Bay Area, China. *Atmosphere* **2020**, *11*, 323. [\[CrossRef\]](#)
32. AIRS Science Team; Teixeira, J. *AIRS/Aqua L3 Daily Standard Physical Retrieval (AIRS-Only) 1 Degree x 1 Degree V006*; NASA Goddard Space Flight Center, Goddard Earth Sciences Data and Information Services Center: Greenbelt, MD, USA, 2013.
33. Levy, R.; Hsu, C. *MODIS Atmosphere L2 Aerosol Product*; Goddard Space Flight Center: Greenbelt, MD, USA, 2015.
34. Tidblad, J.; Kucera, V. *Report No 51: Technical Manual for the Trend Exposure Programme 2005–2006*; UN/ECE International co-Operative Programme on Effects on Materials, including Historic and Cultural Monuments: Stockholm, Sweden, 2006; p. 26.
35. Tidblad, J. *Report No 58: Technical Manual for the Trend Exposure Programme 2008–2009*; UN/ECE International Co-Operative Programme on Effects on Materials, including Historic and Cultural Monuments: Stockholm, Sweden, 2009; p. 62.

36. Tidblad, J.; Gordon, A. *Report No 69: Technical Manual for the Trend Exposure Programme 2011–2012*; UN/ECE International Co-Operative Programme on Effects on Materials, including Historic and Cultural Monuments: Stockholm, Sweden, 2012; p. 71.
37. Tidblad, J. *Report No 79: Technical Manual for the Trend Exposure Programme 2011–2015*; UN/ECE International Co-Operative Programme on Effects on Materials, including Historic and Cultural Monuments: Stockholm, Sweden, 2016; p. 29.
38. Tidblad, J. *Report No 84: Technical Manual for the Trend Exposure Programme 2017–2018*; UN/ECE International Co-Operative Programme on Effects on Materials, including Historic and Cultural Monuments: Stockholm, Sweden, 2018; p. 32.
39. Kreislova, K.; Knotkova, D.; Kvapil, J.; Divisova, H. *Report No. 53: Results from the Multi-Pollutant Programme Corrosion Attack on Carbon Steel after 1 Year of Exposure (2005–2006)*; UN/ECE International Co-Operative Programme on effects on Materials, including Historic and Cultural Monuments: Prague, The Czech Republic, 2008; p. 26.
40. Reiss, D.; Faller, M. *Report 54: Results from the 2005–2006 Trend Exposure Programm. Corrosion Attack of Zinc after 1 Year of Exposure*; UN/ECE International Co-Operative Programme on Effects on Materials, including Historic and Cultural Monuments: Dübendorf, Switzerland, 2007; p. 16.
41. Yates, T. *Report 55: Results from the 2005–2006 Trend Exposure Programm. Corrosion Attack of Limestone after 1 Year of Exposure*; UN/ECE International Co-Operative Programme on Effects on Materials, including Historic and Cultural Monuments: Watford, UK, 2007; p. 9.
42. Lombardo, T.; Ionescu, A. *Report No 59: Soiling of Exposed Materials and Dose-Response Functions for Modern Glass*; UN/ECE International Co-Operative Programme on Effects on Materials, including Historic and Cultural Monuments: Paris, France, 2009; p. 39.
43. Tidblad, J.; Kreislova, K.; Faller, M.; Yates, T.; Lombardo, T.; Grøntoft, T. *Report No 62: Results of Corrosion and Soiling from the 2008–2009 Exposure Programme for Trend Analysis*; UN/ECE International Co-Operative Programme on Effects on Materials, including Historic and Cultural Monuments: Stockholm, Sweden, 2010; p. 18.
44. Tidblad, J.; Gordon, A.; Kreislova, K.; Faller, M.; De La Fuente, D.; Yates, T.; Verney-Carron, A. *Report No 72: Results of Corrosion and Soiling from the 2011–2012 Exposure Programme for Trend Analysis*; UN/ECE International Co-Operative Programme on Effects on Materials, including Historic and Cultural Monuments: Stockholm, Sweden, 2013; p. 24.
45. Tidblad, J.; Kreislova, K.; Faller, M.; De La Fuente, D.; Yates, T.; Verney-Carron, A. *Report No 78: Results of Corrosion and Soiling from the 2011–2015 Exposure Programme for Trend Analysis*; UN/ECE International Co-Operative Programme on Effects on Materials, including Historic and Cultural Monuments: Stockholm, Sweden, 2016; p. 35.
46. Tidblad, J.; Kreislova, K.; Faller, M.; De La Fuente, D.; Yates, T.; Verney-Carron, A.; Vuorio, T. *Report No 85: Results of Corrosion and Soiling from the 2017–2018 Exposure Programme for Trend Analysis*; UN/ECE International Co-Operative Programme on Effects on Materials, including Historic and Cultural Monuments: Stockholm, Sweden, 2019; p. 21.
47. Roberge, P.R. *Handbook of Corrosion Engineering*, 2nd ed.; McGraw-Hill Education: New York, NY, USA, 2012; ISBN 978-0-07-175037-0.
48. Varotsos, P.A.; Alexopoulos, K.D. *Thermodynamics of Point Defects and Their Relation with Bulk Properties*; Defects in Solids: North Holland, The Netherlands, 1986; Volume 14.
49. Livingston, F.E.; George, S.M. Effect of HNO₃ and HCl on HDO Diffusion on Crystalline D₂O Ice Multilayers. *J. Phys. Chem. B* **1999**, *103*, 4366–4376. [\[CrossRef\]](#)
50. Livingston, F.E.; George, S.M. Diffusion Kinetics of HCl Hydrates in Ice Measured Using Infrared Laser Resonant Desorption Depth-Profiling. *J. Phys. Chem. A* **2001**, *105*, 5155–5164. [\[CrossRef\]](#)
51. Livingston, F.E.; Whipple, G.C.; George, S.M. Diffusion of HDO into Single-Crystal H₂¹⁶O Ice Multilayers: Comparison with H₂¹⁸O. *J. Phys. Chem. B* **1997**, *101*, 6127–6131. [\[CrossRef\]](#)
52. Livingston, F.E.; Whipple, G.C.; George, S.M. Surface and Bulk Diffusion of HDO on Ultrathin Single-Crystal Ice Multilayers on Ru(001). *J. Chem. Phys.* **1998**, *108*, 2197–2207. [\[CrossRef\]](#)
53. Livingston, F.E.; Smith, J.A.; George, S.M. Depth-Profiling and Diffusion Measurements in Ice Films Using Infrared Laser Resonant Desorption. *Anal. Chem.* **2000**, *72*, 5590–5599. [\[CrossRef\]](#) [\[PubMed\]](#)
54. Livingston, F.E.; Smith, J.A.; George, S.M. General Trends for Bulk Diffusion in Ice and Surface Diffusion on Ice. *J. Phys. Chem. A* **2002**, *106*, 6309–6318. [\[CrossRef\]](#)
55. Krasnopoler, A.; George, S.M. Infrared Resonant Desorption of H₂O from Ice Multilayers. *J. Phys. Chem. B* **1998**, *102*, 788–794. [\[CrossRef\]](#)
56. Varotsos, C.A.; Zellner, R. A New Modeling Tool for the Diffusion of Gases in Ice or Amorphous Binary Mixture in the Polar Stratosphere and the Upper Troposphere. *Atmos. Chem. Phys.* **2010**, *10*, 3099–3105. [\[CrossRef\]](#)
57. Johnson, P.N.; Davis, R.A. Diffusivity of Ozone in Water. *J. Chem. Eng. Data* **1996**, *41*, 1485–1487. [\[CrossRef\]](#)
58. Cheung, J.L.; Li, Y.Q.; Boniface, J.; Shi, Q.; Davidovits, P.; Worsnop, D.R.; Jayne, J.T.; Kolb, C.E. Heterogeneous Interactions of NO₂ with Aqueous Surfaces. *J. Phys. Chem. A* **2000**, *104*, 2655–2662. [\[CrossRef\]](#)
59. Diaz, M.; Vega, A.; Coca, J. Correlation for the Estimation of Gas-Liquid Diffusivity. *Chem. Eng. Commun.* **1987**, *52*, 271–281. [\[CrossRef\]](#)

60. Varotsos, C.A.; Cracknell, A.P. Remote Sensing Letters Contribution to the Success of the Sustainable Development Goals—UN 2030 Agenda. *Remote Sens. Lett.* **2020**, *11*, 715–719. [[CrossRef](#)]
61. Varotsos, C.; Cartalis, C. Re-evaluation of surface ozone over Athens, Greece, for the period 1901–1940. *Atmos. Res.* **1991**, *26*, 303–310. [[CrossRef](#)]

Disclaimer/Publisher’s Note: The statements, opinions and data contained in all publications are solely those of the individual author(s) and contributor(s) and not of MDPI and/or the editor(s). MDPI and/or the editor(s) disclaim responsibility for any injury to people or property resulting from any ideas, methods, instructions or products referred to in the content.